CO$_2$ Storage Site Analysis, Screening, and Resource Estimation for Cenozoic Offshore Reservoirs in the Central Gulf of Mexico

Xitong Hu [1], Rupom Bhattacherjee [2], Kodjo Botchway [1], Jack C. Pashin [3], Goutam Chakraborty [1] and Prem Bikkina [2,*]

1 Spears School of Business, Oklahoma State University, Stillwater, OK 74078, USA; xitong.hu@okstate.edu (X.H.); kodjo.botchway@okstate.edu (K.B.); goutam.chakraborty@okstate.edu (G.C.)
2 School of Chemical Engineering, Oklahoma State University, Stillwater, OK 74078, USA; rupom.bhattacherjee@okstate.edu
3 Boone Pickens School of Geology, Oklahoma State University, Stillwater, OK 74078, USA; jack.pashin@okstate.edu
* Correspondence: prem.bikkina@okstate.edu

Abstract: The storage potential of hydrocarbon reservoirs in the central Gulf of Mexico (GOM) makes future development of CO$_2$ storage projects in those areas promising for secure, large-scale, and long-term storage purposes. Focusing on the producing and depleted hydrocarbon fields in the continental slope of the central GOM, this paper analyzed, assessed, and screened the producing sands and evaluated their CO$_2$ storage potential. A live interactive CO$_2$ storage site screening system was built in the SAS® Viya system with a broad range of screening criteria combined from published studies. This offers the users a real-time assessment of the storage sites and enables them to adjust the filters and visualize the results to determine the most suitable filter range. The CO$_2$ storage resources of the sands were estimated using a volumetric equation and the correlation developed by the National Energy Technology Laboratory (NETL). The results of this study indicate that 1.05 gigatons of CO$_2$ storage resources are available in the developed reservoirs at the upper slope area of the central GOM. The Mississippi Canyon and Green Canyon protraction areas contain the fields with the largest storage resources.

Keywords: offshore CO$_2$ storage; CO$_2$ EOR; CO$_2$ storage screening system; central Gulf of Mexico; data management; storage resource

1. Introduction

As part of the Regional Carbon Storage Partnership program sponsored by the U.S. Department of Energy (DOE), the Southeast Regional Carbon Storage Partnership (SECARB) focuses on large-scale, long-term CO$_2$ injection and storage evaluation within the southeast United States. An earlier study, the Southeastern Offshore Storage Resource Assessment (SOSRA), assessed the Eastern Gulf and the easternmost portion of the Central Gulf, including two other planning areas: the Mid-Atlantic and the South-Atlantic. Significant advances in knowledge and technology were made in their research for the assessment and quantitative determination of offshore CO$_2$ storage resources in the SOSRA region, which paved the way for commercialization [1].

Previous detailed studies have shed light on multi-phase tectonic history, salt tectonics, stratigraphic and structural petroleum trapping, and multi-stage petroleum systems in the Eastern and Central GOM planning areas [2–6]. Storage potential was also estimated, and more than 100 gigatons of CO$_2$ storage potential were identified in the continental shelf offshore of Mississippi, Alabama, and Florida [6–8]. However, the storage potential of the active and depleted hydrocarbon fields in the central GOM, continental shelf, and continental slope offshore of Louisiana is still largely unknown, and the suitability of the fields for long-term CO$_2$ storage is yet to be investigated.

Oil fields are maturing in the Gulf of Mexico's continental slope, and several fields are undergoing water floods [9–11]. As these fields mature further, advancing to CO_2-enhanced oil recovery may be a viable solution to prolong the life of the fields. The goal of this DOE-funded study is to carry out a high-level assessment of the suitability of the active and depleted fields in the continental slope region of the central GOM for CO_2 storage and estimate the volume of CO_2 that can be stored in the reservoirs on a field-by-field and reservoir-by-reservoir basis. This involves analyzing the subsurface conditions of the fields in the study area, identifying and modifying screening criteria, and applying them to locate potential storage sites. To ease the process of collecting, processing, and analyzing a large volume of geological and production data from the study area and creating user interactive visualizations that provide insights on the potential CO_2 storage sites in the study area, an online cloud platform called SAS® Viya was utilized. SAS® Viya (V.03.05) provides software-driven decision support systems that are well-suited for multi-source, multi-variate, data mining and data analytics problems related to geologic CO_2 storage projects [12], and the use of this software is novel and can be applied to geologic storage problems in sedimentary basins around the world. This online cloud platform also provides a comprehensive solution to integrate different data sources and discover new insights with quick analytics and visualization.

In the scope of this study, the major geological characteristics of continental slope areas of the central GOM were examined and compared to define the appropriate reservoir screening criteria, drawing on the experience of previous regional CO_2 storage assessment and screening studies [13–15]. The 2018 Sands Atlas, published online by the Bureau of Ocean Energy Management (BOEM), was the primary data source used to analyze the study area. A live and interactive CO_2 storage site screening system was built in the SAS® Viya platform that allows users to change the criteria to screen and visualize the locations of potential reservoirs quickly in the central GOM. In addition, ArcGIS® Pro was used as a supplementary tool for geospatial analysis and analysis of geological features.

High-level estimation of CO_2 storage resources of the reservoirs in the study area is also provided using the static volumetric equations from Smith et al. [15] and the National Energy Technology Laboratory (NETL) [16]. The density of CO_2 under reservoir conditions was estimated as a function of pressure and temperature using the correlation developed by Bikkina et al. [17] and incorporated in the storage estimation. These estimations are used in the SAS® Viya system to identify fields with the optimum CO_2 storage resource.

It should be noted that the estimation of CO_2 storage resources should also include current economic and regulatory considerations [16]. Even though deepwater fields in the eastern portion of the study area were prioritized in storage estimation due to their proximity to the Mississippi Delta shoreline and the associated infrastructure, assessing factors such as the cost of operation, transport to the storage site, injection, and well maintenance is beyond the scope of this study and not considered in the estimation. Thus, according to the CO_2 Storage Resources Management System (SRMS) guidelines by Society of Petroleum Engineer (SPE) (SPE) [18], the estimated storage potential falls into the category of contingent storage resource and is assumed to be equal to the SRMS storage capacity until more information about the regulatory logistics and economic feasibility of offshore storage operations becomes available.

2. Study Area

The active and depleted oil and gas reservoirs in the GOM are located in federal offshore areas off the southeast coasts of Texas, Louisiana, Mississippi, Alabama, and Florida. There are 1317 unique fields and 13,380 sands reported in the 2018 BOEM Sands Atlas database, out of which 862 fields (5500 sands) are depleted. This study focuses only on the active and depleted oil and gas fields in the central GOM, including all federal and state waters east of the Lafayette District to the Mobile and Viosca Knoll areas at the eastern boundary (Figure 1).
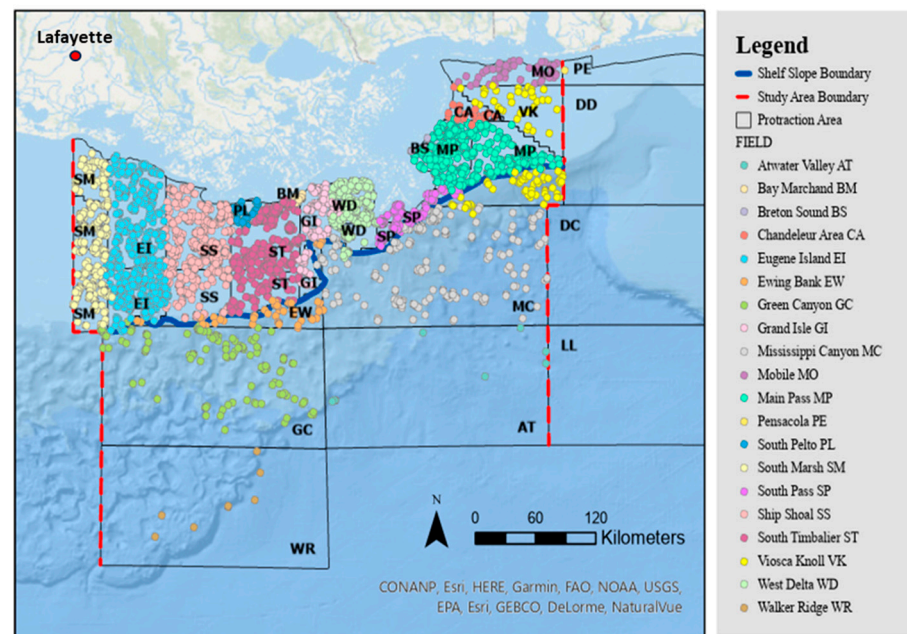
Figure 1. Well location map of the SECARB offshore area. Wells were classified into shelf area and slope area by shelf–slope boundary (dark blue line). Sand body information is from the Bureau of Ocean and Energy Management's 2018 Sands Atlas (https://www.data.boem.gov/Main/GandG.aspx (accessed on 2 September 2021)).

From the offshore Louisiana continental shelf to the upper continental slope, the study area was classified into shelf and slope zones. The study area includes 672 unique fields and 7496 data points from reservoir sands. In the region, 509 fields (6537 sands) are in the shelf region, and 163 fields (956 sands) are in the slope region (Table 1). The shelfbreak follows the northern margin of the Ewing Bank, Mississippi Canyon, and southern Viosca Knoll areas (blue line, Figure 1).

Table 1. Number of depleted and active fields/reservoir sands in the central GOM.

Region	Field Status	Fields	Sands
Shelf	Active	207	4940
	Depleted	302	1597
	Total	509	6537
Slope	Active	114	838
	Depleted	50	118
	Total	163	956
Grand Total		672	7493

The CO_2 storage reservoir screening system and the CO_2 storage potential assessment employed in this study focused on the slope area, and the sands are distributed at the south and southeast of the shelf–slope boundary in Ewing Bank, Mississippi Canyon, Southern Viosca Knoll, Green Canyon, Atwater Valley, and Walker Ridge protraction areas (Table 2). The slope region fields in the eastern portion of the study area (i.e., Southern Viosca Knoll and Mississippi Canyon protraction areas) were prioritized in storage estimation (Section 4.4) due to their proximity to the shoreline and the associated infrastructure. These fields require offshore transportation infrastructure for the development of CO_2 storage and CO_2-EOR sites.

Table 2. Protraction areas and number of fields/sands in the upper slope region of the study area.

Protraction Areas	Status	Fields	Sands
Atwater Valley AT	Active	2	9
	Depleted	4	5
Ewing Bank EW	Active	13	138
	Depleted	5	10
Green Canyon	Active	34	253
	Depleted	13	31
Mississippi Canyon MC	Active	44	340
	Depleted	19	53
Viosca Knoll VK	Active	14	76
	Depleted	9	19
Walker Ridge WR	Active	7	22
Grand Total		164	956

Previous studies revealed that saline formations and hydrocarbon reservoirs in the study area were strongly affected by salt tectonics. On the Louisiana Shelf, reservoir strata were deposited above allochthonous salt that accumulated above an Oligocene–Miocene detachment. Strata are complexly faulted and dominated by Roho structures and associated diapiric salt bodies [19,20]. The upper continental slope contains a variety of allochthonous salt bodies developed above a system of ramps and flats that rise southward from the Mesozoic section into the Pleistocene–recent section. This area contains numerous allochthonous salt bodies and turbidite mini-basins with reservoirs distributed throughout the mini-basins [21–24]. Reservoirs consist of turbidite channel-fan deposits, and reservoir sands include a complex mosaic of channel, levee, proximal fan, and distal fan deposits [25–27].

3. Methodology

3.1. Dataset

The data used in this assessment are primarily from the Bureau of Ocean Energy Management's (BOEM) 2018 Sands Atlas (https://www.data.boem.gov/Main/GandG.aspx) (accessed on 2 September 2021) and include detailed information on individual wells and their productive sands in the central GOM. Sand names in the BOEM database are unique and associated with a play number and field name. Thus, each sand is essentially the individual reservoir in each field. Production data for each sand are provided in the database, assuming that the sands are not in communication with each other. Therefore, structures and reservoir properties are also assumed to be distinct for each sand and should reflect distinct storage resources for each reservoir. The ranges of values for some of the parameters obtained from the BOEM database for the sands from our study area are listed in Table 3. The important sand attributes available for each sand body include sand location, subsea depth, water depth, sand thickness, initial temperature, initial pressure, porosity, permeability, water saturation, and hydrocarbon production information (e.g., original oil in place, original gas in place, original barrel of oil equivalent (BOE), etc.).

Table 3. Reservoir properties from the BOEM database for our study area.

	Shelf	Slope
Sand Counts	6537	956
Average Subsea Depth (feet)	8971.12 (2734.40 m)	13,100.97 (3993.18 m)
Average Thickness (feet)	21.75 (6.63 m)	38.29 (11.67 m)
Average Area (acres)	581.29 (2.35 km^2)	901.33 (3.65 km^2)
Average Temperature (°F)	183.49 (84.16 °C)	169.17 (76.21 °C)

Table 3. *Cont.*

	Shelf	**Slope**
Average Pressure (psi)	5056.42 (34.86 mPa)	8599.45 (40.68 mPa)
Average Porosity	0.28	0.29
Average Permeability (mD)	391.03	589.56
Average Water Saturation	0.28	0.25
Average Original Barrel of Oil Equivalent (BOE) (bbl)	3,895,682.04 (619.36 million L)	14,682,604.78 (2334.35 million L)

3.2. CO_2 Density Estimation

An accurate estimation of CO_2 density is required to understand the state of CO_2 in the reservoir condition and choose the storage sites that will allow the injected CO_2 to be stored in the reservoir in the supercritical state. CO_2 density is also an important parameter to estimate storage resources using the correlation developed by NETL [16]. In this study, CO_2 density was estimated at the initial reservoir conditions using the prediction method developed by Bikkina et al. [17] and compared (Figure 2) with the predictions from the National Institute of Standards and Technology (NIST) database [28,29]. The temperature and pressure ranges of the prediction method from Bikkina et al. [17] are 53.5 °F (12 °C) to 212 °F (100 °C) and 1 to 600 bars, respectively. In general, the predictions from Bikkina et al. [17] were very similar to the NIST predictions, even for the temperature and pressure values that exceed the limit of the method (Figure 2). The mean absolute error (MAE) between the two methods was 0.013 g/cm^3, and the root mean square deviation (RMSD) was 0.015 g/cm^3. It should also be mentioned that the NIST methodology is applicable to the density of pure CO_2, whereas Bikkina et al. [17] assumed the CO_2 to be saturated with water, which offers a better approximation of the state of CO_2 after injection into the reservoir. Hence, the densities estimated by Bikkina et al. [17] were used in this study for site screening and storage estimation, discussed in Sections 3.3 and 3.4.
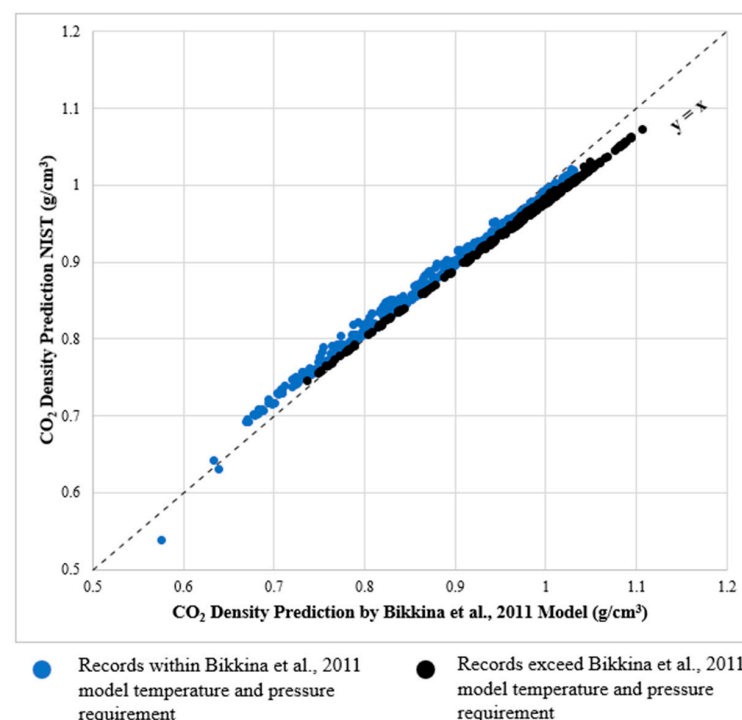

Figure 2. CO_2 density prediction by Bikkina et al. [17] vs. NIST method. Blue markers represent the CO_2 prediction of the sands within the Bikkina et al. [17] pressure and temperature model prediction range, and grey color markers are the CO_2 density predictions that exceed the Bikkina et al. [17] model prediction range.

3.3. CO$_2$ Storage Sites Screening Criteria

In this study, the reservoir screening criteria of Raza et al. [30], developed for depleted gas reservoirs, and Smith et al. [15], primarily defined for CO$_2$-EOR, were combined with the screening criteria proposed for the study area using the analysis of the geologic attributes (temperature, pressure, porosity, permeability, and API gravity) and the published geologic studies in the region [4,22,23,31,32].

The main aspects considered for screening CO$_2$ storage sites were storage capacity, injectivity, trapping mechanism, and containment. Reservoir temperature, pressure, and CO$_2$ density play big roles in determining the storage capacity of the reservoirs. Denser supercritical CO$_2$ occupies a smaller pore volume, allowing maximum pore volume utilization and mobility across the reservoir. The density of CO$_2$ increases with depth, which is why many studies have reported that efficient storage takes place in sites that are at least 800 m deep [33–38]. The porosity of the reservoir, which decreases with depth, should also be high enough to ensure maximum storage capacity. There are other aspects, such as the geometry of depositional facies, the buoyancy of CO$_2$, and irreducible water saturation, that can also affect the efficiency of storage capacity [37,39,40]. However, these factors were not considered in this study due to a lack of data.

The injectivity of reservoirs depends on how well the injected fluid can flow through the stratigraphic intervals. This aspect is mainly controlled by the reservoir pressure, permeability, and thickness. Low permeability and thin reservoir intervals adversely affect the CO$_2$ injectivity. Studies have revealed that reservoirs with high (>100 mD) near wellbore permeability require a lesser number of injection wells for favorable injection [41]. Increased reservoir pressure with CO$_2$ injection can also limit the injectivity and storage capacity due to excessive pressure buildup, especially for reservoirs with natural water drive [42,43]. Bachu [44] reported a 3% decrease in storage capacity in oil and gas reservoirs supported by weak water drive. Other factors that can affect CO$_2$ injectivity in oil and gas reservoirs but were not considered in this study include mineral dissolution or precipitations due to geochemical reactions between rocks and fluids.

Screening the reservoirs on the aspects of trapping mechanism is very tricky because, depending on the type of trapping, a lot of physico-chemical and geological properties such as reservoir temperature, pressure, CO$_2$–Brine/H$_2$O interfacial tension, rock wettability, capillary pressure, viscosity, geometry of pores, etc., may impact storage [14,45–48]. In the scope of this study and keeping the availability of data in mind, only reservoir temperature, pressure, and rock type were considered for screening. Reservoir pressure and temperature affect the density of CO$_2$ and the rate at which CO$_2$ plumes migrate upward [49]. Reservoir conditions also affect the dissolution of CO$_2$ into the formation fluid. CO$_2$ solubility in formation fluid increases with pressure and decreases with temperature and salinity of formation water [50].

Seal geometry (lateral continuity and thickness) and hydraulic integrity of the reservoirs are the key aspects of storage site containment [39]. Hydrocarbon accumulation without associated seeps in the studied sands indicates seal integrity of the caprocks in the reservoirs. However, seal integrity might change due to the increase in pore pressure upon CO$_2$ injection. A significant increase in the pore pressure might cause mechanical breakdown of the seals [51,52]. Therefore, the hydraulic integrity of the reservoir must also be considered during site screening. Reservoirs that are normally pressured to weakly over-pressured are optimal for CO$_2$ storage. The integrity of the seal also depends on its thickness. Different studies have suggested different cut-off numbers for seal thickness. Ramírez et al. [53] suggested that seals should have at least 10 m of thickness to prevent cross-formational flow of CO$_2$, whereas Raza et al. [30] proposed 100 m as the minimum seal thickness for depleted gas reservoirs. Published geological studies in the central GOM region indicate numerous shale intervals in the Miocene–Pleistocene section between 50 and 100 m thick [4,22,23,31,32]. Many normal faults exist within the slope minibasins, and these faults pose the greatest risk for cross-formational flow, particularly where original

reservoir pressure approaches fracture pressure. Indeed, joints are largely absent in Gulf of Mexico mudrocks, and documented seeps are commonly along faults and salt margins [54].

3.4. CO_2 Storage Estimation Methods

The primary method used for CO_2 storage estimation is the method provided by the U.S. Department of Energy's National Energy Technology Laboratory [16], referred to as the NETL method in this study. The CO_2 storage efficiency factor ($E_{oil/gas}$) was chosen as 15%, 25%, and 40% for low (P_{10}), medium (P_{50}), and high (P_{90}) resource estimations, respectively. These efficiency factor values were considered based on the fact that the sands in continental slope areas tend to be more homogenous, and the experience from water flooding shows that recovery could approach 40% in some of the fields [55]. The equation is provided below:

$$G_{CO_2} = Ah_n\varphi_e\left(1 - S_{wi}\right)B\rho_{CO_2}E_{oil/gas},$$

where

G_{CO_2} = mass estimate of oil and gas reservoir CO_2 storage resource, unit *: M;

A = area that defines the oil or gas reservoir that is being assessed for CO_2 storage, unit *: L^2;

h_n = net oil and gas column height in the reservoir, unit *: L;

φ_e = average effective porosity **;

S_{wi} = average initial water saturation within the reservoir unit *: L^3/L^3;

B = fluid formation volume factor, unit *: L^3/L^3;

ρ_{CO_2} = density of CO_2 evaluated at reservoir pressure and temperature, unit *: M/L^3;

$E_{oil/gas}$ = CO_2 storage efficiency factor, the volume of CO_2 stored in an oil or gas reservoir per unit volume of original oil or gas in place (OOIP or OGIP), unit *: L^3/L^3;

* L = length; M = mass.

** The studied sands have good permeability, so the average effective porosities are assumed to be equal to the average porosities of the sands.

In addition, the volumetric method [15] was also used to estimate CO_2 storage resources and then compared with those calculated using the NETL method [16]. Generally, the volumetric method estimates the theoretical maximum storage resource of the reservoir. It should also be noted that these storage estimation methods are static and do not differentiate between different trapping potentials. Mechanisms such as the dissolution of CO_2 into brines [56] or crude oil and mineralization [57] can increase the estimated storage resource, which was not considered in this study. An integrated reservoir model coupled with wellbore and reservoir properties would provide a more robust estimation of CO_2 storage resources and reservoir behavior within the fields as well as help understand other dynamics of CO_2 storage, such as trapping mechanisms, injectivity, and plume migration [58]. The following are the CO_2 storage resource estimation functions from Smith et al. [15] for the volumetric method:

$$Q = AT\varphi\rho_{CO_2}\left(1 - S_w\right),$$

where

Q = storage resource of the oil reservoir, tonne (metric) CO_2;

A = field area, m^2;

T = producing interval thickness, m;

φ = average reservoir porosity, %;

ρ_{CO_2} = density of CO_2, g/cc;

$1 - S_w$ = saturation of oil, where S_w is the initial reservoir water saturation, %.

4. Results and Discussion

4.1. Key Screening Criteria Comparison between Shelf and Upper Slope

4.1.1. Reservoir Temperature and Pressure

One of the critical screening criteria in the identification of suitable CO_2 storage reservoirs is the reservoir temperature. In general, the temperature vs. subsea depth plot of the slope (Figure 3) area shows a relatively strong positive 0.67 Pearson correlation between the two parameters, impacted by the cooling effect of the water column over a broad range of seabed depth (718 m to 9388 m), as well as thermal effects associated with salt bodies.
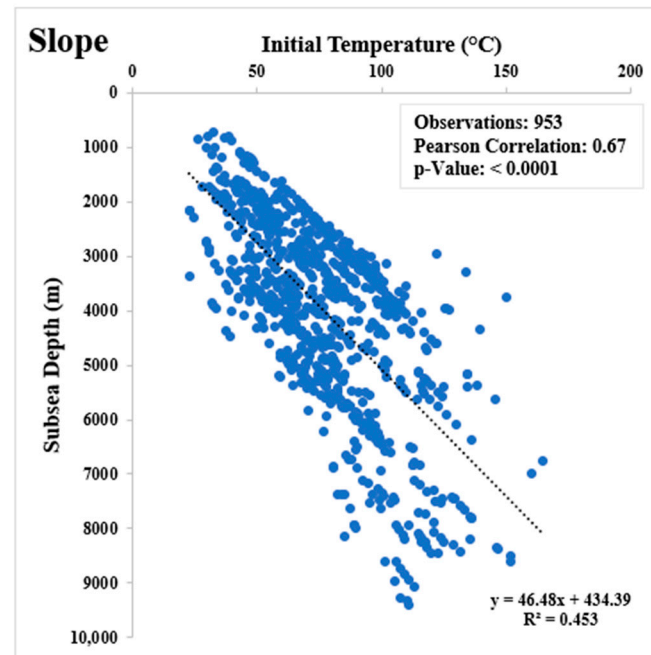
Figure 3. Initial temperature vs. subsea depth in the slope area.

To better understand the initial temperature distribution of the slope sands, the initial temperature and the subsea depth of the sand by the well location were examined (Figure 4). The initial temperatures of the slope sands ranged from 22.8 °C (73 °F) to 164.4 °C (328 °F), while sand subsea depths ranged from 718 m (2355 ft) to 9388 m (30,800 ft). As illustrated by the initial temperature vs. subsea depth correlation plot (Figure 3), low-temperature sands generally correspond with lesser subsea depth, while high-temperature sands generally correspond with greater subsea depths (larger bubble size). Broadly, the spatial distribution of sands shows that a cluster of higher temperature sands is located near the northwest and north margin of the Mississippi Canyon and southern Viosca Knoll protraction areas, as well as associated with some deep wells in the Mississippi Canyon, Green Canyon, Ewing Bank, and Walker Ridge protraction areas (Figure 4).

The sand temperature gradient map (Figure 5) shows a gradual decrease in the temperature gradient from the shelf–slope boundary down to the slope area except in the Walker Ridge (WR) area, where the temperature gradient slightly increased compared to the temperature gradients of the sands in the Green Canyon (GC) and Atwater Valley (AT) protraction areas.

In addition to reservoir temperature, reservoir pressure is also critical for the identification of suitable CO_2 storage sites. Figure 6 shows a strong and statistically significant Pearson correlation between initial pressure and subsea depth for the slope area. The observations are below the lithostatic gradient of 22.6 KPa/m (1.0 psi/foot) but mostly higher than the hydrostatic gradient of 9.8 KPa/m (0.433 psi/ft) in the slope area based on the initial reservoir temperature and pressure conditions. Reservoirs below lithostatic pressure gradient have a high potential for storage because there is considerable headroom

for injection without stressing the reservoir. The headroom for injection increases as the pressure depletes with the production of hydrocarbons.
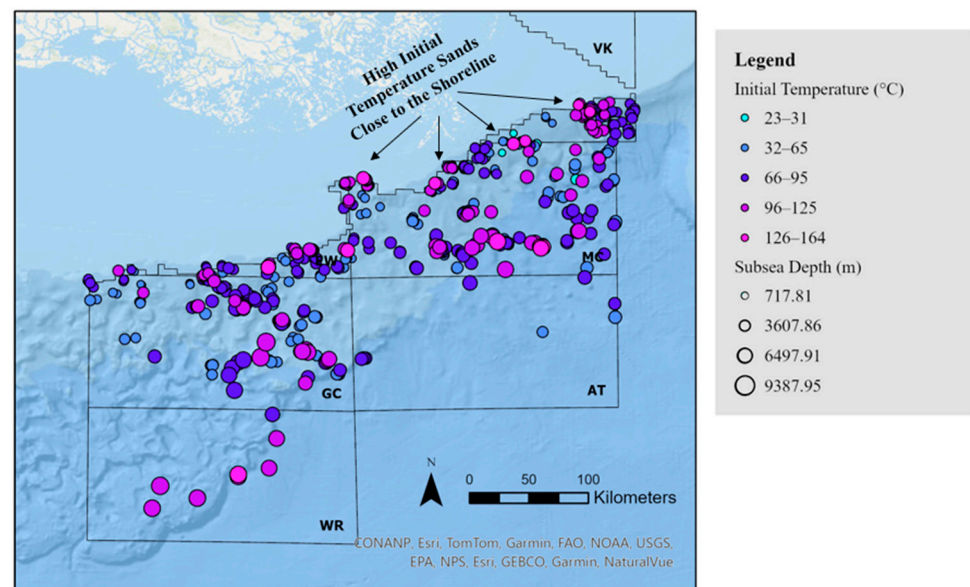

Figure 4. Initial temperature and subsea depth of the sands in the slope zone. Note that color shade corresponds to initial temperature while symbol size corresponds to subsea depth (m).
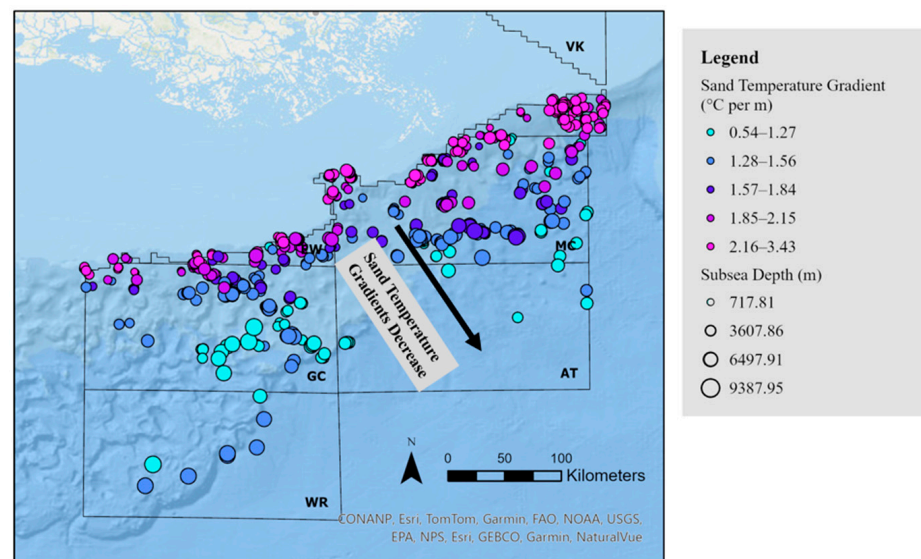

Figure 5. The temperature gradient and subsea depth of the sands in the slope zone. The general temperature gradient shows a decreasing trend from the shelf–slope boundary to the slope Green Canyon (GC) and Atwater Valley (AT) area.

Maximum initial reservoir pressure reaches 148,989 kPa in the slope area. The spatial distribution of initial pressure and subsea reservoir depth (Figure 7) also reveals a positive correlation between the initial reservoir pressure and subsea depth. High-pressure sands (yellow and orange colors, 72,010–148,989 kPa) are located in the southern and southeast of the slope area. The initial pressure of sands close to the shelf–slope boundaries is relatively low (dark color, 8094–33,116 kPa).
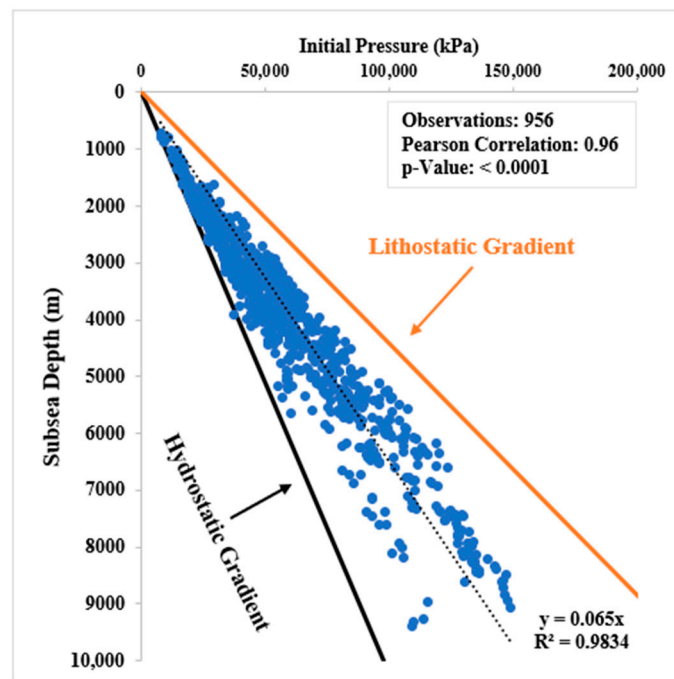
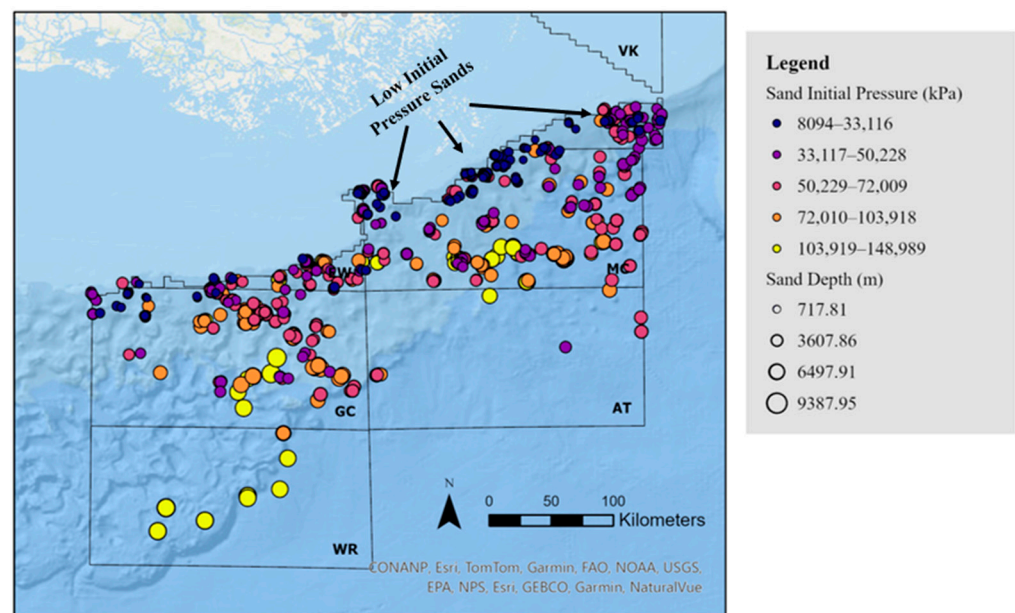**Figure 6.** Initial reservoir pressure vs. subsea depth in the slope area.

Figure 7. The initial pressure and subsea depth of the slope sands.

The pressure–depth quotient map (Figure 8) shows the pressure–depth gradient of each sand. Here, the yellow and green colors indicate that the sands have initial pressure–depth quotients (15.5–19.3 kPa/m) close to the lithostatic gradient and thus little headroom for CO_2 injection prior to hydrocarbon production. These high-pressure–depth quotient sands are scattered throughout the region. The dark purple color indicates that reservoirs with relatively low initial pressure–depth quotients (9.5–12.2 kPa/m) are distributed especially at the northwest corner and north margin of Mississippi Canyon, and few sands are at the east margin of the south Viosca Knoll, indicating significant headroom for injection. The headroom is even higher in reservoirs that have been depressurized by hydrocarbon production.
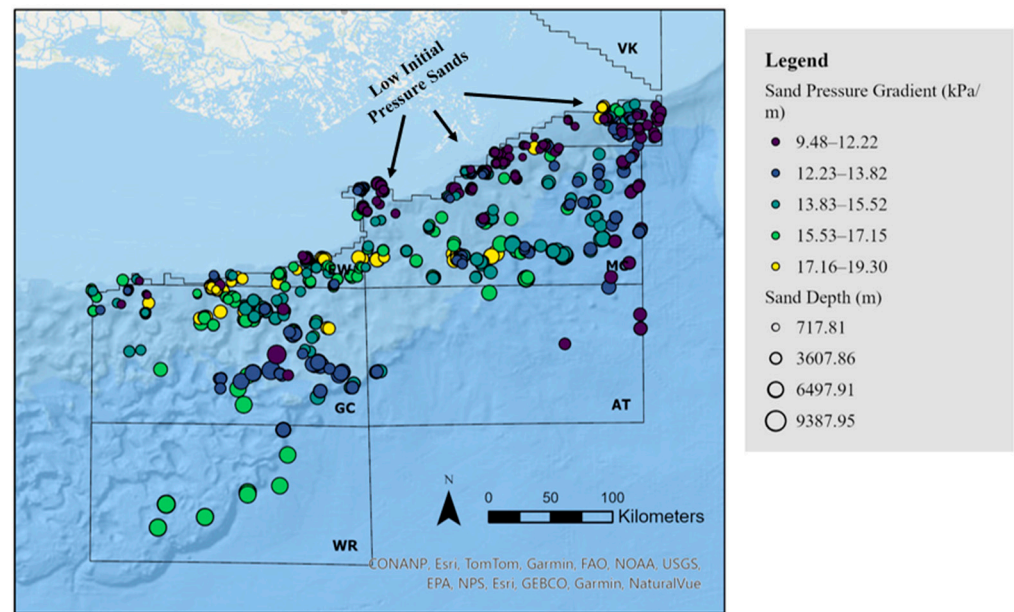
Figure 8. The pressure–depth quotient map of the slope sands. Dark purple color represents low-pressure–depth gradient sands and the yellow color indicates the sands that are close to the lithostatic gradient. It is important to note that sands near the hydrostatic gradient have significant headroom for CO_2 injection.

From the initial temperature and initial pressure spatial distribution map of the sands in the slope area (Figure 9), it is observed that northern boundary sands generally have high initial temperatures with relatively low pressures (pink, light pink, and purple colors). Conversely, a number of sands located in the Green Canyon, Walker Ridge, and Mississippi Canyon areas are in high initial pressure conditions with correspondingly high initial temperatures (deep blue color).
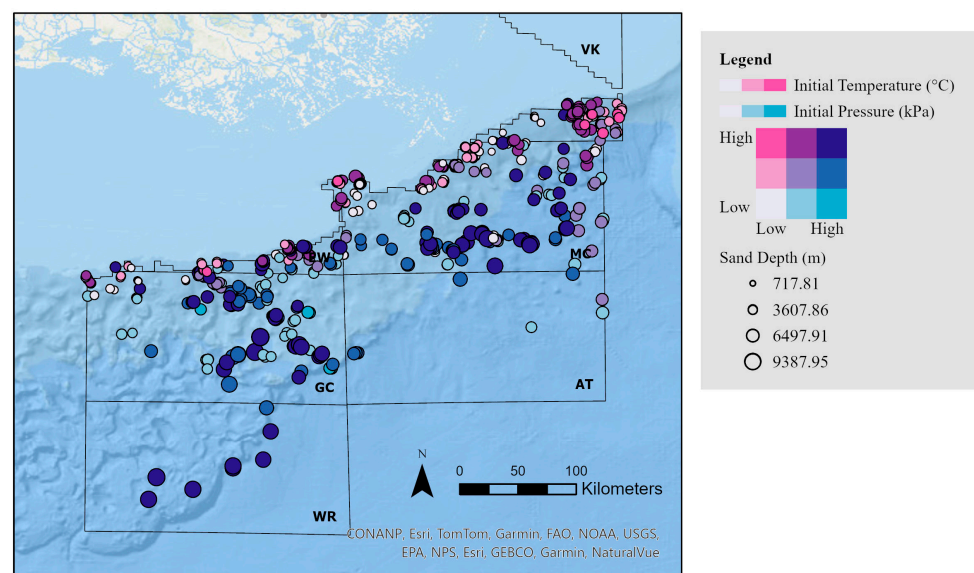

Figure 9. The initial pressure and initial temperature of the sands in the slope zone. Bubble size indicates sand depth, and bubble color indicates the relative initial pressure and relative initial temperature. Low temperature to medium temperature boundary is 64.4 °C, and medium temperature to high temperature boundary is 86.1 °C. Low pressure to medium pressure boundary is 43,154 kPa, and medium pressure to high pressure boundary is 64,390 kPa.

However, when interpreting our findings, it is important to keep in mind that the initial temperature and pressure values utilized in our study to characterize the storage sites may not be reflective of the conditions in the mature reservoir state. Pressure depletion is an issue, although the shut-in pressure tests indicate rapid pressure rebound. Cooling of mature reservoirs by fluid flow and adiabatic gas expansion is probably a factor, but no data on mature reservoir temperature were found. Accordingly, original pressures and temperatures appear adequate for assessment, but pressure decline/recovery characteristics and mature reservoir temperature should be considered when considering pilot programs and injection design.

4.1.2. Reservoir Porosity and Permeability

Porosity and permeability influence the total volume of CO_2 that can be stored and the rate at which CO_2 can be injected into a given reservoir. For data from slope areas, porosity and permeability semi-log scale plots show a positive and statistically significant linear relationship (Figure 10). Porosity values appear to cluster between 20% and 35%, while permeability values are commonly greater than 100 mD. It is important to note that Darcy-class permeability was also observed in the slope area, so reservoir properties are regionally favorable for CO_2 storage.
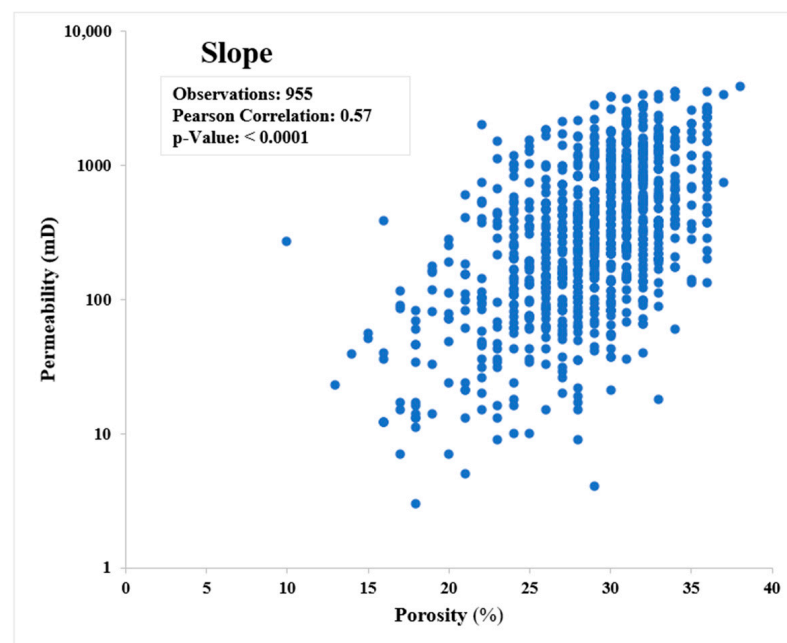

Figure 10. Porosity vs. permeability (log scale) for sands located in the slope area.

In addition, the porosity–permeability distribution map (Figure 11) shows that most of the sands are in favorable porosity and permeability range (deep blue color, >20% porosity and >100 mD permeability). Some sands with good porosity but low permeability are also scattered in the slope region (pink color, >20% porosity and <100 mD permeability). Only a few sands have unfavorable porosity and permeability conditions for CO_2 storage in the slope area (white color, <20% porosity and <100 mD permeability).

4.1.3. Gas–Oil Ratio and API Oil Gravity

Plotting the gas–oil ratio vs. API gravity in slope reservoirs in the SECARB offshore area (Figure 12) reveals that most reservoirs have gas–oil ratios between 0.4 and 10. Where the gas–oil ratio exceeds 100, oil gravity is commonly not reported. In general, a low gas–oil ratio favors the sweep of hydrocarbons by injection of CO_2. Miscible CO_2 flooding is possible where API gravity is between 22° and 48°, but values between 30° and 40° are commonly considered optimal [59].
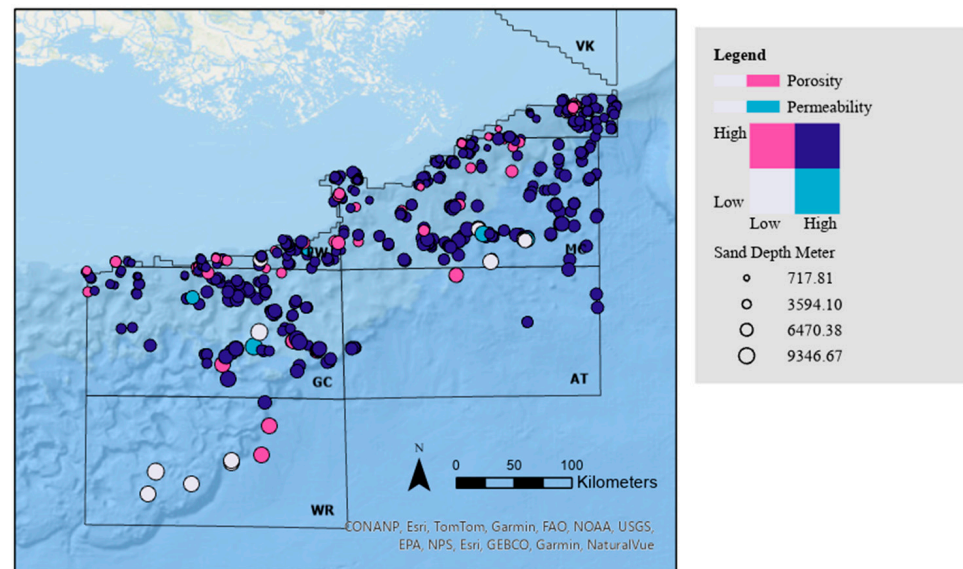
Figure 11. Porosity and permeability of the sands in the slope area. Overall, 20% is the low and high boundary of the porosity, and 100 mD is the low–high boundary of permeability. Most of the sands in the slope area are within the high porosity and high permeability boundary (dark blue color), which is favorable for CO_2 storage.
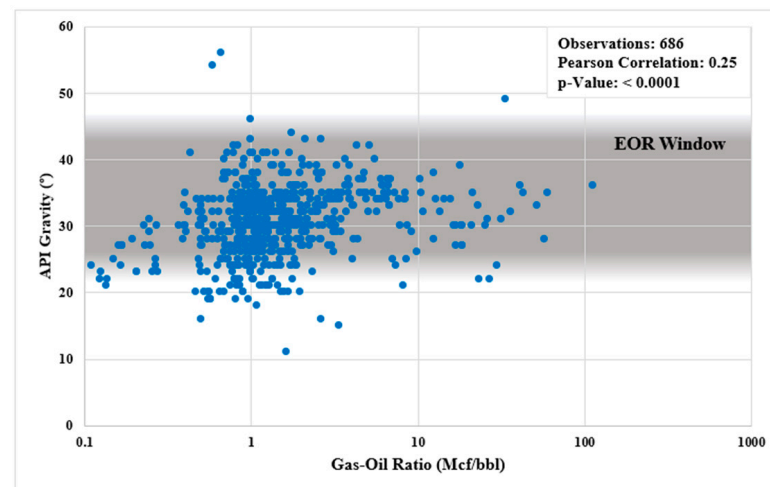

Figure 12. Plot of gas–oil ratio (log scale) versus API gravity for oil-rich slope reservoirs in the SECARB offshore project area.

4.2. Screening Criteria

After studying the data and combining the screening criteria from Raza et al. [53] and Smith et al. [15], a total of 10 screening criteria were proposed and applied to screen sands in this study (Table 4). These factors reflect the storage capacity, injectivity, solubility trapping, capillary trapping, and containment aspects of CO_2 storage sites.

Due to the scope of the study, other CO_2 storage screening criteria, including lateral continuity of the seal, thickness of the seal, and secondary recovery phase of the reservoir, were not applied.

Table 4. Screening criteria applied in this study.

Parameters	Positive Indicators	Indication Aspect
Subsea Depth	$\geq$2304 feet (702 m)	Storage Capacity
Porosity	$\geq$20%	Storage Capacity Capillary Trapping
Permeability	$\geq$100 mD	Injectivity
Initial Reservoir Temperature	>CO_2 critical temperature (304.13 K, 31.0 °C, 87.8 °F)	Storage Efficiency
Pressure	>CO_2 critical pressure (7.3773 MPa, 72.8 atm, 1070 psi, 73.8 bar)	Storage Efficiency
Pressure–Depth Quotients	<15.5 KPa/m (0.68 psi/ft)	Injectivity
API Gravity	22°–48° feasible (medium-light crude oil); 30°–40° considered optimal (light crude oil) [59]	Injectivity
Cumulative Production	$\geq$10,000 barrels (1.59 million L)	Storage Potential
Rock Type	Quartz-rich sandstone, typically poorly consolidated	Capillary Trapping
CO_2 Density	>0.6 g/cc	Storage Capacity

4.3. CO_2 Storage Site Screening Platform

The SAS® Viya Explore and Visualization interface provides excellent functionality for building the CO_2 storage screening platform. A total of 6537 observations (the unique sand bodies in each BOEM field) from the shelf area and 956 observations from the slope area were mapped in SAS® Viya. The filter function provides easy handling of the observations based on the attributes. The range of the value distribution for each variable appears along the number axis of that filter, and the user can filter the values in real-time using slider bars. Several important screening criteria are included in the reservoir screening platform in SAS® Viya (Figure 13, right-hand portion). In addition to the filter function, users can specify the color and size of the marker and label attributes to visualize the observations.
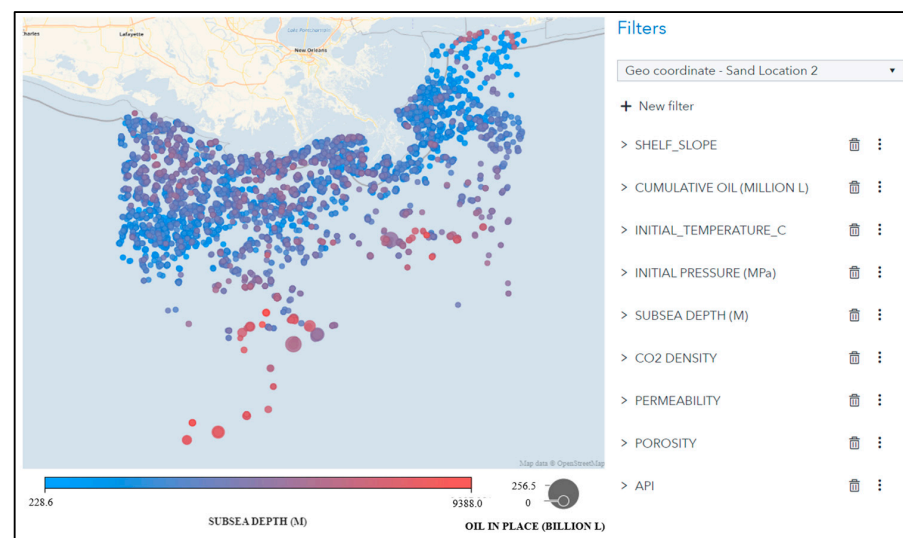

Figure 13. SECARB offshore CO_2 storage screening platform. Blue color and red color represent the subsea depth of the sand, and symbol size corresponds to original oil in place (OOIP).

The SAS® Viya platform is highly interactive and enables visualization of the data through the map view. Additionally, filters can be adjusted to display screening criteria in real-time. Users may quickly change the criterion ranges to fit a given purpose with a series of sliders. Figure 14 shows the distribution of the sands in the slope area (956 sands).

For the 956 sands in the slope area, the counts of filtered sands are listed in Table 5 with the corresponding screening criteria. Over 308 sands were filtered out in order to meet the API gravity range between 22°–48°. In addition, 212 sands were filtered due to less than 10,000 barrels of cumulative production, and 186 sands were filtered out because of less than 100 mD permeability. After applying all screening criteria, the original 956 sands were filtered down to 445 sands in the slope area. Most of the filtered sands are found

in the Mississippi Canyon, Green Canyon, and Viosca Knoll areas. The CO_2 storage site screening criteria filters and corresponding ranges are displayed in Figure 15.
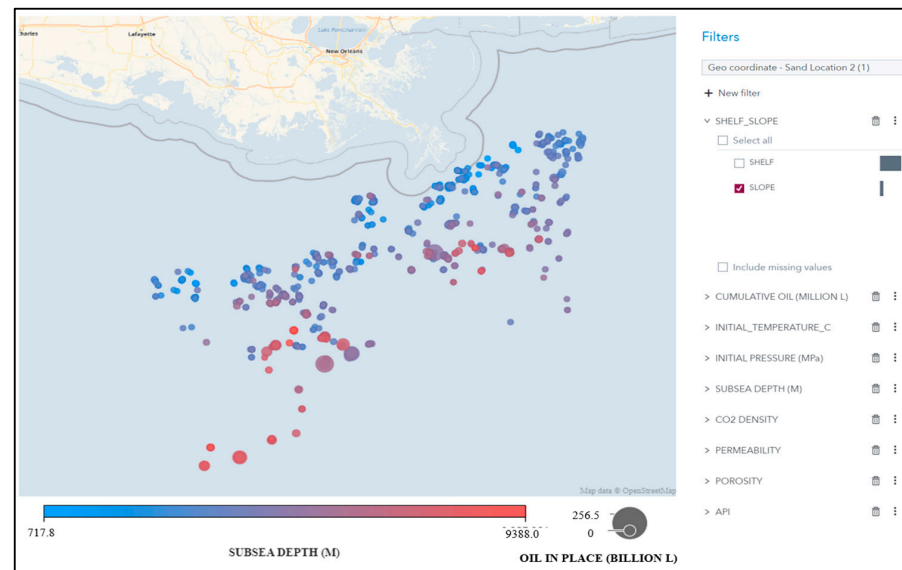

Figure 14. Distribution of sands in the slope color-coded by subsea depth. Size correlates to original oil in place (OOIP).

Table 5. The counts of satisfied sands and filtered sands in the slope area with corresponding screening criteria.

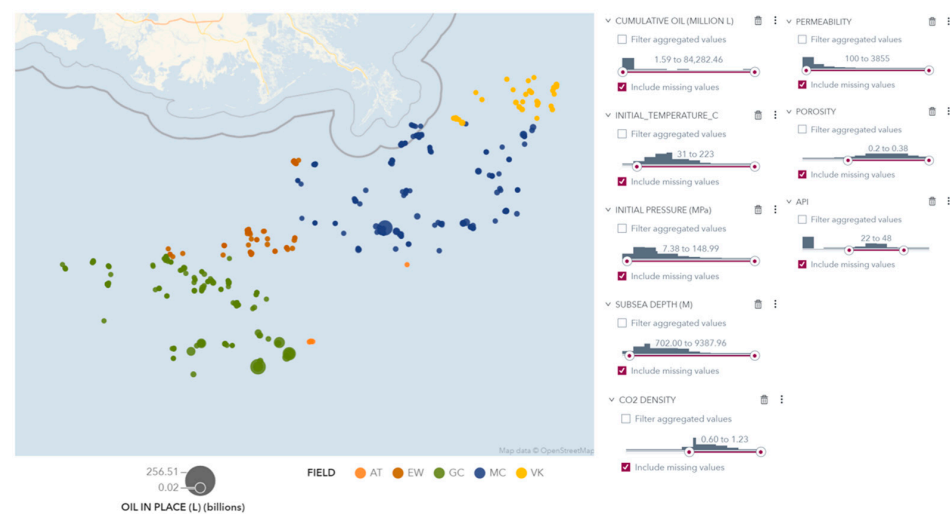| Screening Criteria	Satisfied Sands	Filtered Sands
Cumulative Oil ($\geq$1.59 million L, 10,000 bbl)	744	212
Initial Temperature ($\geq$31.1 °C, 87.98 °F)	942	14
Initial Pressure ($\geq$7.3773 MPa, 1070 psi)	956	0
Subsea Depth ($\geq$702 m, 2304 feet)	956	0
CO2 Density (>0.6 g/cc)	955	1
Permeability ($\geq$100 mD)	770	186
Porosity ($\geq$20%)	919	37
Oil API Gravity (22°–48°, API units)	648	308
All Conditions	445	511

Figure 15. The remaining 445 slope sands after applying the screening criteria defined in Table 4 of this study.

4.4. CO_2 Storage Estimation

After applying the screening criteria established in Table 1 to the sands in the slope area, the CO_2 storage estimations were recalculated following the NETL method. The estimated storage capacity (NETL P_{50}) of the screened BOEM fields in the slope area is 1.05 gigatons in total (445 satisfied sands in Table 5).

Table 6 shows the top 10 CO_2-estimated storage BOEM fields. MC807 is the highest CO_2 storage target, with an estimated 68% more storage resources than the second-ranked field (GC743). A total of four fields in the slope area have an estimated P_{50} storage capacity greater than 50 Mt.

Table 6. The top ten BOEM fields from slope area in terms of estimated CO_2 storage resources.

BOEM Field	NETL Method—Low (P10), Eoil/Gas = 15% (Megatons)	NETL Method—Medium (P50), Eoil/Gas = 25% (Megatons)	NETL Method—High (P90), Eoil/Gas = 40% (Megatons)	Volumetric Method Storage Resource (Megatons)
MC807	108	181	289	1052
GC743	64	107	171	543
GC826	59	98	158	451
GC640	53	88	141	456
GC654	29	48	77	221
MC776	22	37	59	206
MC778	17	28	45	154
MC084	17	28	44	151
GC562	13	21	34	117
MC696	10	17	27	90

As discussed in Section 2, close proximity to the Mississippi Delta may allow for the less costly development of fields located in the Mississippi Canyon and Viosca Knoll protraction areas. Table 7 provides an account of the estimated CO_2 storage resources for the top 10 fields from these two protraction areas, and Figure 16 shows the location of the top 10 fields in the Mississippi Canyon and Visco Knoll protraction areas.

Table 7. The top ten BOEM fields in terms of estimated CO_2 storage resources are from Mississippian Canyon and Viosca Knoll protraction areas.

BOEM Field	NETL Method—Low (P$_{10}$), Eoil/Gas = 15% (Megatons)	NETL Method—Medium (P$_{50}$), Eoil/Gas = 25% (Megatons)	NETL Method—High (P$_{90}$), Eoil/Gas = 40% (Megatons)	Volumetric Method Storage Resource (Megatons)
MC807	108	181	289	1052
MC776	22	37	59	206
MC778	17	28	45	154
MC084	17	28	44	151
MC696	10	17	27	90
MC194	10	16	25	112
VK956	10	16	25	142
MC935	8	14	22	71
VK990	8	13	21	80
MC383	8	13	20	75

Among the 10 fields, MC807 is the highest-ranked field with over 150 Mt storage resources based on the NETL P_{50} estimation method. The remaining fields in these two protraction areas have an estimated NETL P_{50} storage resource of less than 50 Mt. The corresponding reservoir sizes and geological conditions for these fields are provided in Tables 8 and 9, respectively.
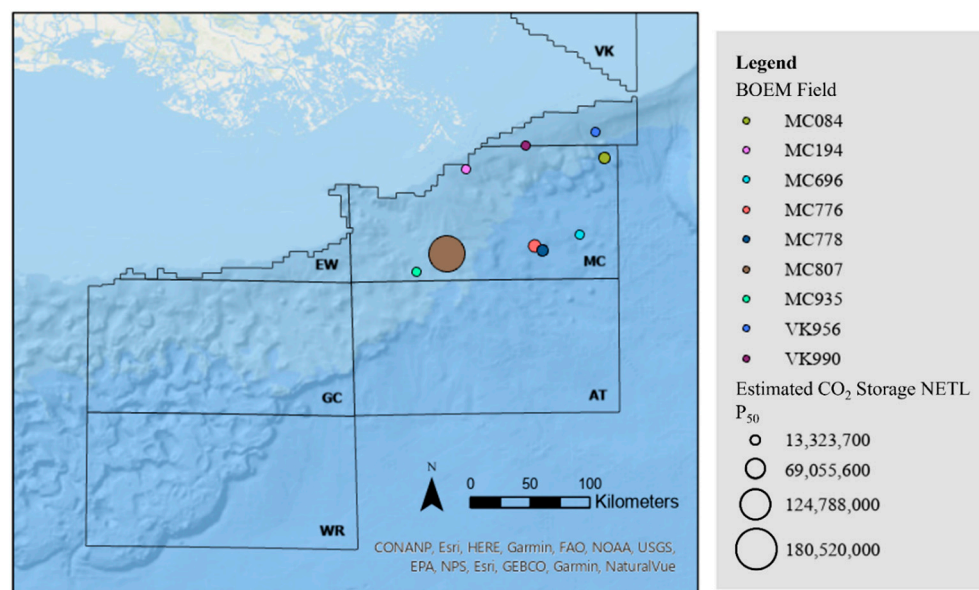
Figure 16. The top ten BOEM fields in terms of estimated CO_2 storage resources are from Mississippian Canyon and Viosca Knoll protraction areas.

Table 8. The reservoir sizes of the top ten BOEM fields from Table 7.

BOEM Field	Count of Sands	NETL Medium Storage Resource (P_{50}) (Megatons)	Total Area (km^2)	Average Area (km^2)	Average Reservoir Thickness (m)	Average Subsea Depth (m)
MC807	26	181	325.59	17.34	16.47	5144
MC776	4	37	25.07	8.69	34.71	6047
MC778	7	28	48.30	9.55	17.74	6822
MC084	6	28	51.88	11.99	19.85	4028
MC696	4	17	24.89	8.62	15.06	7003
MC194	8	16	65.29	11.31	6.81	2622
VK956	4	16	85.03	29.47	7.80	3783
MC935	3	14	18.29	8.44	22.53	5272
VK990	8	13	36.75	6.35	7.69	2331
MC383	2	13	22.74	15.76	11.58	3812

Table 9. The geological conditions of the top ten BOEM fields from Table 7.

BOEM Field	Average Initial Reservoir Pressure (MPa)	Average Initial Reservoir Temperature (°C)	Average Permeability (mD)	Average Porosity	Average Water Saturation	Total OOIP (Billion L)	Total ROIP (Billion L)
MC807	80.71	76.28	491.12	0.29	0.20	148.25	7.20
MC776	92.39	92.64	1062.50	0.27	0.16	54.80	1.45
MC778	107.90	115.39	653.71	0.23	0.15	68.63	2.01
MC084	50.42	75.65	511.00	0.27	0.20	114.38	11.60
MC696	104.79	111.25	902.25	0.25	0.18	706.68	67.82
MC194	32.71	59.93	497.13	0.32	0.29	52.67	1.39
VK956	49.16	99.44	688.25	0.29	0.19	124.71	6.62
MC935	86.03	73.33	441.67	0.27	0.22	58.16	0.01
VK990	31.36	56.74	422.38	0.31	0.29	49.27	0.91
MC383	54.77	63.06	2266.00	0.34	0.18	49.64	2.03

One explanation for the high estimated storage resource of the MC807 block is the advanced field development (26 sand bodies across most of the block) in this block (Table 8). The other high-ranking blocks in the Mississippi Canyon and Viosca Knoll areas completed fewer than 10 producing sand bodies, and the well patterns are much more localized than in MC807. Importantly, many of the field areas estimated by BOEM are based on the current state of development rather than the overall size of the oil accumulation, and refined estimates of potential productive areas are being delineated seismically and may result in a significant expansion of the storage resource.

To further rank the CO_2 storage resource, the CO_2 storage resource per unit area was calculated using SAS® Viya. Here, the estimated CO_2 storage resource for each sand was divided by the productive area specified by BOEM, and the data were aggregated at the field level. Table 10 lists the top-ranked fields in the Mississippi Canyon and Viosca Knoll areas based on storage resource (NETL P_{50} estimation method) per unit area (km^2). Notably, the 10 highest-ranked fields are all from the Mississippi Canyon protraction area and the MC776 field has the highest storage resource per unit area (estimated P_{50} = 1.48 Mt/km^2). Table 11 provides an overview of the reservoir conditions for each of these fields.

Table 10. The top ten BOEM fields in terms of storage resources per unit area from Mississippi Canyon and Viosca Knoll and corresponding reservoir size.

BOEM Field	Count of Sands	NETL Medium (P_{50}) Storage Resource per Unit Area (Megatons/km^2)	Total Area (km^2)	Average Area (km^2)	Average Reservoir Thickness (m)	Average Subsea Depth (m)
MC776	4	1.48	25.07	6.27	34.71	6047
MC029	1	1.32	0.45	0.45	28.91	2932
MC899	3	0.93	9.91	3.30	22.86	4951
MC698	1	0.90	3.53	3.52	20.64	4886
MC935	3	0.77	18.30	6.10	22.53	5272
MC696	4	0.68	24.89	6.22	15.08	7002
MC800	1	0.63	0.70	0.70	17.81	4833
MC682	1	0.61	12.86	12.86	26.05	7520
MC778	7	0.59	48.30	6.90	17.74	6821
MC807	26	0.55	325.59	12.52	16.47	5144

Table 11. Geological characteristics of the top ten BOEM fields from Table 10.

BOEM Field	Reservoir Pressure (MPa)	Reservoir Temperature (°C)	Permeability (mD)	Porosity	Water Saturation	Total OOIP (Billion L)	Total ROIP (Billion L)
MC776	92.39	92.64	1062.50	0.27	0.16	932	45
MC029	86.03	73.33	441.67	0.27	0.22	15	0.3
MC899	104.79	111.25	902.25	0.25	0.18	228	20
MC698	107.90	115.40	653.71	0.23	0.15	86	8
MC935	80.71	76.28	491.12	0.29	0.20	345	9
MC696	54.77	63.06	2266.00	0.34	0.18	432	13
MC800	50.42	75.65	511.00	0.27	0.20	11	0.3
MC682	28.53	55.83	891.50	0.30	0.20	195	8
MC778	54.53	70.00	1009.88	0.30	0.20	719	73
MC807	57.34	61.67	392.71	0.30	0.28	4445	427

It should be noted that this study aimed to provide a high-level static assessment of the suitability of the studied sands for CO_2 storage. The estimated storage resources are theoretical maximum and do not take different trapping mechanisms, plume geometry, and plume dynamics into consideration, which may affect the storage potential. For example, the dissolution of injected CO_2 into the formation fluid can increase the storage resource estimated with NETL or volumetric methods. The dynamics of CO_2 at subsurface

conditions can also alter this estimated storage resource. For example, if the buoyancy force exerted by the formation fluid is higher than the sealing capillary pressure, the injected CO_2 can migrate to the seal rock and eventually escape from the storage site, affecting the storage potential. Hence, to further assess the storage capacity of the sands, a detailed investigation of different types of trapping potentials of the sands and how the injected CO_2 would behave in the subsurface formation in the presence of other fluids should be considered in future studies.

An opportunity exists to prolong the life of the oil fields in the continental slope through CO_2-enhanced oil recovery with associated storage, and the success of waterflooding operations in increasing recovery and growing reserves is promising for the technology. Several logistical factors need to be considered, and careful thought and reservoir modeling efforts are required to design a system of injection and production wells, determine optimal well spacing, and organize well patterns to minimize the risk of cross-formational flow along faults. For example, aligning producers between injectors and faults will help minimize the risk of pressure buildup and flow of CO_2 into fault systems. Obtaining CO_2 supply is another challenge, and pipelines and shipping appear to be the most viable options. Limited platform space is a factor that challenges the implementation of waterflood operations [11], and so the same hurdle challenges the implementation of CO_2-enhanced recovery operations. Other challenges include installing corrosion-resistant tubing strings in wells that are CO_2-ready and installing recycle loops for reinjection of CO_2 that is co-produced with the oil. Meeting these challenges will prolong the life of deepwater fields while contributing substantially to greenhouse gas reduction goals in the region.

5. Conclusions

In this study, the SAS® Viya platform was utilized to manage geological datasets and analyze the geological characteristics of the sands in shelf and slope areas through the use of correlation plots and sand feature distribution maps. In the slope area, the pressure and temperature show a linear positive correlation to depth. The porosity vs. permeability plot shows the sands in the slope area typically have 20–35% porosity and permeability greater than 100 mD, which indicates favorable objectives for CO_2 injection. Most of the sands in the continental slope have a gas–oil ratio of less than 10 Mcf/bbl and 22°–48° API gravity that is favorable for CO_2-EOR.

A series of screening criteria to characterize the hydrocarbon reservoirs and analyze their CO_2 storage and EOR potential were defined. Reservoir properties, fluid properties, and production history were considered in the design of the system. Ten screening criteria were employed. The SAS® Viya platform was used to filter data from 956 sand bodies in the slope area. The screening procedure identified 445 reservoirs prospective for CO_2 injection in the existing fields, which are mainly in the Green Canyon, Mississippi Canyon, and Viosca Knoll protraction areas.

Storage estimation revealed that at a regional level, after applying the screening criteria, 1.05 gigatons of CO_2 storage resources (NETL P50 estimation method) are available in the developed reservoirs in the continental slope area. The fields with the largest overall projected CO_2 storage resource were found in the Mississippi Canyon protraction area. Therefore, near-term development initiatives may seek to focus efforts in the Mississippi Canyon area because of its close proximity to the Mississippi Delta and large estimated CO_2 storage resources. Even though the Green Canyon has fields with high geologic storage potential (Tables 3 and 4), it is not a good candidate for CO_2 storage; the shelf is highly faulted, which limits reservoir size, and the Green Canyon lies offshore across the shelf and thus requires installation of infrastructures like pipelines to reach.

Due to their proximity to the Delta, the Mississippi Canyon and Viosca Knoll protraction areas were examined in more detail. For these two protraction areas, the top ten fields had an estimated CO_2 storage resource of 363 Mt (NETL P50 estimation method). Importantly, of the fields analyzed in the Mississippi Canyon and Viosca Knoll protraction areas, the top ten most prospective fields (based on P50 estimations storage per unit

area) are located in the Mississippi Canyon area. This observation suggests that future developmental activities may benefit from focusing efforts in the Mississippi Canyon area.

It is also noteworthy that the considerable amount of storage resources in the Mississippi Canyon makes it "low-hanging fruit" for near-term CO_2 storage, given the in-place platform infrastructure and, potentially, usable pipelines. However, expansion into non-hydrocarbon bearing reservoirs (i.e., saline reservoirs) proximal to the oil accumulations is a logical next step. Hence, using traditional geological workflows coupled with data mining, future studies can evaluate storage resources beyond/below the oil–water contact.

Data Availability Statement: Publicly available datasets were analyzed in this study. This data can be found here: https://www.data.boem.gov/Main/GandG.aspx (accessed on 2 September 2021).

Conflicts of Interest: The authors declare no conflicts of interest.

References

1. Nemeth, K.; Sams-Gray, K.; Berry, P.; Ripepi, N.; Pashin, J.; Knapp, J.; Hills, D.; Riestenberg, D. *Southeast Offshore Storage Resource Assessment (SOSRA)(Final Technical Report)*; Southern States Energy Board: Peachtree Corners, GA, USA; Virginia Polytechnic Inst. and State Univ.(Virginia Tech): Blacksburg, VA, USA; Oklahoma State Univ.: Stillwater, OK, USA; Geological Survey of Alabama: Tuscaloosa, AL, USA; Advanced Resources International: Knoxville, TN, USA, 2019.
2. Galloway, W.E. Depositional Evolution of the Gulf of Mexico Sedimentary Basin. In *Sedimentary Basins of the World 5*; Elsevier: Amsterdam, The Netherlands, 2008; pp. 505–549.
3. Pashin, J.C.; Jin, G.; Hills, D.J. Mesozoic structure and petroleum systems in the DeSoto Canyon salt basin in the mobile, Pensacola, Destin Dome, and Viosca Knoll areas of the MAFLA shelf. In Proceedings of the 35th Annual Gulf Coast Section SEPM (GCSSEPM) Foundation Bob F. Perkins Research Conference, Houston, TX, USA, 4–6 December 2016; pp. 315–340.
4. Bouroullec, R.; Weimer, P.; Serrano, O. Petroleum geology of the Mississippi Canyon, Atwater Valley, western DeSoto Canyon, and western Lloyd Ridge protraction areas, northern slope Gulf of Mexico: Traps, reservoirs, and tectono-stratigraphic evolution. *AAPG Bull.* **2017**, *101*, 1073–1108. [CrossRef]
5. Meng, J.; Pashin, J.C.; Nygaard, R.; Chandra, A. Analysis of the stress field in the DeSoto canyon Salt Basin for ensuring safe offshore carbon storage. *Int. J. Greenh. Gas Control* **2018**, *79*, 279–288. [CrossRef]
6. Meng, J.; Pashin, J.C.; Chandra, A.; Xue, L.; Sholanke, S.; Spears, J. Structural framework and fault analysis in the east-central Gulf of Mexico shelf: Implications for offshore CO_2 storage. *J. Struct. Geol.* **2020**, *134*, 104020. [CrossRef]
7. Hills, D.J.; Pashin, J.C. *Preliminary Assessment of Offshore Transport and Storage of CO2: Southeastern Regional Carbon Sequestration Partnership Final Report*; Southern States Energy Board: Peachtree Corners, GA, USA, 2010; Volume 11.
8. Chandra, A. Geological Characterization and CO_2 Storage Potential of Cretaceous Sandstone in the DeSoto Canyon Salt Basin of the MAFLA Shelf. Master's Thesis, Oklahoma State University, Stillwater, OK, USA, 2018.

9. Tallin, A.G.; Cowan, K.M.; MacEachern, D.P.; Roes, V.; Schnitker, S. A Fitness for Purpose Assessment of the Use of a Modified Expandable Casing Patch as Barrier Against H2S Exposure. AADE-05-NTCE-21. In Proceedings of the Paper Presented to the American Association of Drilling Engineers 2005 National Technical Conference and Exhibition, Houston, TX, USA, 5–7 April 2005.

10. Wilson, A. Waterflooding Proves Useful in Deepwater Gulf of Mexico Overpressured Turbidites. *J. Pet. Technol.* **2014**, *66*, 113–115. Available online: https://jpt.spe.org/waterflooding-proves-useful-deepwater-gulf-mexico-overpressured-turbidites (accessed on 12 June 2023). [CrossRef]

11. Priest, T. *Shell Oil's Deepwater Mission to Mars*; University of Iowa Press: Iowa City, IA, USA, 2019; p. 108.

12. Bhattacherjee, R.; Botchway, K.O.; Hu, X.; Pashin, J.; Chakraborty, G.; Bikkina, P. *Evaluating CO$_2$ Storage Potential of Offshore Reservoirs and Saline Formations in Central Gulf of Mexico by Employing Data-Driven Models with SAS® Viya*; Western Users of SAS Software: San Francisco, CA, USA, 2022.

13. Aminu, M.D.; Nabavi, S.A.; Rochelle, C.A.; Manovic, V. A review of developments in carbon dioxide storage. *Appl. Energy* **2017**, *208*, 1389–1419. [CrossRef]

14. Raza, A.; Rezaee, R.; Bing, C.H.; Gholami, R.; Hamid, M.A.; Nagarajan, R. Carbon dioxide storage in subsurface geologic medium: A review on capillary trapping mechanism. *Egypt. J. Pet.* **2016**, *25*, 367–373. [CrossRef]

15. Smith, S.A.; Sorensen, J.A.; Steadman, E.N.; Harju, J.A.; Fischer, D.W. Estimates of CO$_2$ storage capacity in selected oil fields of the northern Great Plains region of North America. *AAPG Stud. Geol.* **2009**, *59*, 87–97.

16. Goodman, A.; Hakala, A.; Bromhal, G.; Deel, D.; Rodosta, T.; Frailey, S.; Small, M.; Allen, D.; Romanov, V.; Fazio, J.; et al. US DOE methodology for the development of geologic storage potential for carbon dioxide at the national and regional scale. *Int. J. Greenh. Gas Control* **2011**, *5*, 952–965. [CrossRef]

17. Bikkina, P.K.; Shoham, O.; Uppaluri, R. Equilibrated interfacial tension data of the CO$_2$-water system at high pressures and moderate temperatures. *J. Chem. Eng. Data* **2011**, *56*, 3725–3733. [CrossRef]

18. Frailey, S.; Koperna, G.; Tucker, O. The CO$_2$ Storage Resources Management System (SRMS): Toward a Common Approach to Classifying, Categorizing, and Quantifying Storage Resources. In Proceedings of the 14th Greenhouse Gas Control Technologies Conference Melbourne, Rochester, NY, USA, 21–26 October 2018; pp. 21–26.

19. Diegel, F.A.; Karlo, J.F.; Schuster, D.C.; Shoup, R.C.; Tauvers, P.R. Cenozoic structural evolution and tectonostratigraphic framework of the northern Gulf Coast continental margin. *AAPG Mem.* **1995**, *65*, 109–151.

20. Rowan, M.G.; Jackson MP, A.; Trudgill, B.D. Salt-related fault families and fault welds in the northern Gulf of Mexico. *AAPG Bull.* **1999**, *83*, 1454–1484.

21. Hudec, M.R.; Jackson, M.P.A.; Shultz-Ela, D.D. The paradox of minibasin subsidence into salt: Clues to the evolution of crustal basins. *Geol. Soc. Am. Bull.* **2009**, *121*, 201–221. [CrossRef]

22. Bouroullec, R.; Weimer, P. Geometry and kinematics of Neogene allochthonous salt systems in the Mississippi Canyon, Atwater Valley, western Lloyd Ridge, and western DeSoto Canyon protraction areas, northern, deep-water Gulf of Mexico. *AAPG Bull.* **2017**, *101*, 1003–1034. [CrossRef]

23. Sholanke, S. Structural Framework Analysis in the Mississippi Canyon Protraction Area, Central Gulf of Mexico: Implications for CO$_2$ Sequestration. Master's Thesis, Oklahoma State University, Stillwater, OK, USA, 2020; p. 98.

24. Godec, M.; Jalali, J.; Koperna, G.; Hill, G.; Oudinot, A.; Pashin, J.; Riestenberg, D.; Wernette, B. *Parametric Study to Assess Technical Prospect Feasibility for Offshore CO$_2$ Storage*; White Paper, U.S. Department of Energy contract DE-FE0031557; Southern States Energy Board: Peachtree Corners, GA, USA, 2020; p. 47.

25. Mahaffie, M.J. Reservoir Classification for Turbidite Intervals at the Mars Discovery, Mississippi Canyon 807, Gulf of Mexico. In *Submarine Fans and Turbidite Systems: Sequence Stratigraphy, Reservoir Architecture, and Production Characteristics-Gulf of Mexico and International, Proceedings of the 15th Annual Gulf Coast SEPM Research Conference, Houston, TX, USA, 4–7 December 1994*; Weimer, P., Bouma, A.H., Perkins, B.F., Eds.; Society for Sedimentary Geology: Tulsa, OK, USA, 1994; pp. 233–244.

26. Meckel, L.; Ugueto, G.; Lynch, H.; Cumming, E.; Hewett, B.; Bocage, E.; Winker, C.; O'Neill, B. Genetic Stratigraphy, Stratigraphic Architecture, and Reservoir Stacking Patterns of the Upper Miocene—Lower Pliocene Greater Mars–Ursa Intraslope Basin, Mississippi Canyon, Gulf of Mexico. In *Sequence Stratigraphic Models for Exploration and Production: Evolving Methodology, Emerging Models, and Application Histories: 22nd Annual Gulf Coast Research Conference*; Society for Sedimentary Geology: Tulsa, OK, USA, 2002; pp. 113–147.

27. Ewing, T.E.; Galloway, W.E. Evolution of the Northern Gulf of Mexico Sedimentary Basin. In *Sedimentary Basins of United States and Canada*, 2nd ed.; Miall, A.D., Ed.; Elsevier: Amsterdam, The Netherlands, 2019; pp. 627–694.

28. Span, R.; Wagner, W. A new equation of state for carbon dioxide covering the fluid region from the triple-point temperature to 1100 K at pressures up to 800 MPa. *J. Phys. Chem. Ref. Data* **1996**, *25*, 1509–1596. [CrossRef]

29. Lemmon, E.; Eric, W.; Ian, H.; Huber, M.L.; Mclinden, M.O. *NIST Standard Reference Database 23: Reference Fluid Thermodynamic and Transport Properties-REFPROP, Version 10.0*; National Institute of Standards and Technology: Gaithersburg, MD, USA, 2018.

30. Raza, A.; Rezaee, R.; Gholami, R.; Bing, C.H.; Nagarajan, R.; Hamid, M.A. A screening criterion for selection of suitable CO$_2$ storage sites. *J. Nat. Gas Sci. Eng.* **2016**, *28*, 317–327. [CrossRef]

31. Ehrenberg, S.N.; Nadeau, P.H.; Steen, Ø. A mega scale view of reservoir quality in producing sandstones from the offshore Gulf of Mexico. *Am. Assoc. Pet. Geol. Bull.* **2008**, *92*, 145–164.

32. Pashin, J.C.; Spears, J.; Ademilola, J. Sedimentation, structure, and reservoir properties in prospective offshore geologic carbon sinks, Gulf of Mexico, International Association of Sedimentologists. In Proceedings of the 21st International Sedimentological Congress Abstract Book, Beijing, China, 22–26 August 2022; p. 2083.

33. Black, J.R.; Carroll, S.A.; Haese, R.R. Rates of mineral dissolution under CO_2 storage conditions. *Chem. Geol.* **2015**, *399*, 134–144. [CrossRef]

34. Ketzer, J.M.; Iglesias, R.; Einloft, S. Reducing Greenhouse Gas Emissions with CO_2 Capture and Geological Storage. In *Handbook of Climate Change Mitigation and Adaptation*; Chen, W.Y., Suzuki, T., Lackner, M., Eds.; Springer: Cham, Switzerland, 2017; pp. 2197–2237. [CrossRef]

35. Kimbrel, E.H.; Herring, A.L.; Armstrong, R.T.; Lunati, I.; Bay, B.K.; Wildenschild, D. Experimental characterization of nonwetting phase trapping and implications for geologic CO_2 sequestration. *Int. J. Greenh. Gas Control* **2015**, *42*, 1–15. [CrossRef]

36. Metz, B.; Davidson, O.; De Coninck, H.; Loos, M.; Meyer, L. *IPCC Special Report on Carbon Dioxide Capture and Storage*; Cambridge University Press: Cambridge, UK, 2005.

37. Pentland, C.H. Measurements of non-wetting phase trapping in porous media. *Energy Procedia* **2011**, *1*, 3173–3180.

38. Qi, D.; Su, K. Risk Assessment of CO_2 Geological Storage and the Calculation of Storage Capacity. In Proceedings of the 2009 Asia-Pacific Power and Energy Engineering Conference, Wuhan, China, 27–31 March 2009; IEEE: Piscataway, NJ, USA, 2009; pp. 1–4.

39. Ambrose, W.; Lakshminarasimhan, S.; Holtz, M.; Núñez-López, V.; Hovorka, S.D.; Duncan, I. Geologic factors controlling CO_2 storage capacity and permanence: Case studies based on experience with heterogeneity in oil and gas reservoirs applied to CO_2 storage. *Environ. Geol.* **2008**, *54*, 1619–1633. [CrossRef]

40. Solomon, S. Carbon dioxide storage: Geological security and environmental issues–Case study on the Sleipner gas field in Norway. *Bellona Rep.* **2007**, *128*, 27–31.

41. Watson, M.N.; Gibson-Poole, C.M. Reservoir selection for optimised geological injection and storage of carbon dioxide: A combined geochemical and stratigraphic perspective. In Proceedings of the Fourth Annual Conference on Carbon Capture and Storage, Alexandria, Egypt, 2–5 May 2005; National Energy Technology Laboratory, US Department of Energy: Alexandria, Egypt, 2005; pp. 2–5.

42. Ghaderi, S.M.; Keith, D.W.; Leonenko, Y. Feasibility of injecting large volumes of CO_2 into aquifers. *Energy Procedia* **2009**, *1*, 3113–3120. [CrossRef]

43. Jalil, M.; Masoudi, R.; Darman, N.B.; Othman, M. Study of the CO_2 injection, storage, and sequestration in depleted M4 carbonate gas condensate reservoir, Malaysia. In Proceedings of the Carbon Management Technology Conference, Orlando, FL, USA, 7–9 February 2012; OnePetro: Richardson, TX, USA, 2012.

44. Bachu, S. Evaluation of CO_2 sequestration capacity in oil and gas reservoirs in the Western Canada Sedimentary Basin. *Alta. Geol. Surv. Alta. Energy Util. Board March* **2004**, *114*, 1–77.

45. Bachu, S. Screening and Ranking of Hydrocarbon Reservoirs for CO_2 Storage in the Alberta Basin, Canada. In *US Department of Energy–National Energy Technology Laboratory, National Conference on Carbon Sequestration*; Citeseer: Princeton, NJ, USA, 2001; Volume 67.

46. Bandara, U.C.; Tartakovsky, A.M.; Palmer, B.J. Pore-scale study of capillary trapping mechanism during CO_2 injection in geological formations. *Int. J. Greenh. Gas Control* **2011**, *5*, 1566–1577. [CrossRef]

47. Chalbaud, C.; Robin, M.; Lombard, J.-M.; Bertin, H.; Egermann, P. Brine/CO_2 interfacial properties and effects on CO_2 storage in deep saline aquifers. *Oil Gas Sci. Technol. Rev. De L'institut Français Du Pétrole* **2010**, *65*, 541–555.

48. Wildenschild, D.; Armstrong, R.T.; Herring, A.L.; Young, I.M.; Carey, J.W. Exploring capillary trapping efficiency as a function of interfacial tension, viscosity, and flow rate. *Energy Procedia* **2011**, *4*, 4945–4952. [CrossRef]

49. Lu, C.; Han, W.S.; Lee, S.-Y.; McPherson, B.J.; Lichtner, P.C. Effects of density and mutual solubility of a CO_2–brine system on CO_2 storage in geological formations:"Warm" vs."cold" formations. *Adv. Water Resour.* **2009**, *32*, 1685–1702. [CrossRef]

50. Chevalier, G.; Diamond, L.W.; Leu, W. Potential for deep geological sequestration of CO_2 in Switzerland: A first appraisal. *Swiss J. Geosci.* **2010**, *103*, 427–455. [CrossRef]

51. Olden, P.; Pickup, G.; Jin, M.; Mackay, E.; Hamilton, S.; Somerville, J.; Todd, A. Use of rock mechanics laboratory data in geomechanical modelling to increase confidence in CO_2 geological storage. *Int. J. Greenh. Gas Control* **2012**, *11*, 304–315. [CrossRef]

52. Raza, A.; Rezaee, R.; Gholami, R.; Rasouli, V.; Bing, C.H.; Nagarajan, R.; Hamid, M.A. Injectivity and quantification of capillary trapping for CO_2 storage: A review of influencing parameters. *J. Nat. Gas Sci. Eng.* **2015**, *26*, 510–517. [CrossRef]

53. Ramírez, A.; Hagedoorn, S.; Kramers, L.; Wildenborg, T.; Hendriks, C. Screening CO_2 storage options in the Netherlands. *Int. J. Greenh. Gas Control* **2010**, *4*, 367–380. [CrossRef]

54. Hardage, B.A.; Muarray, P.E.; Remington, R.; De Angelo, M.; Sava, D.; Roberts, H.H.; Shedd, W.; Hunt, J., Jr. Multicomponent seismic technology assessment of fluid-gas expulsion geology and gas-hydrate systems. *Am. Assoc. Pet. Geol. Mem.* **2009**, *89*, 247–265.

55. Godec, M.; Jalali, J.; Koperna, G.; Hill, G.; Oudinot, A.; Pashin, J.; Riestenberg, D.; Wallace, M.; Wernette, B. *Characterization of Offshore Storage Resource Potential in the Central Planning Area of the Gulf of Mexico*; Milestone Report, U.S. Department of Energy contract DE-FE0031557; Southern States Energy Board: Peachtree Corners, GA, USA, 2020; p. 96.

56. Bhattacherjee, R.; Botchway, K.; Pashin, J.C.; Chakraborty, G.; Bikkina, P. Machine learning-based prediction of CO_2 fugacity coefficients: Application to estimation of CO_2 solubility in aqueous brines as a function of pressure, temperature, and salinity. *Int. J. Greenh. Gas Control* **2023**, *128*, 103971. [CrossRef]

57. Soong, Y.; Goodman, A.; McCarthy-Jones, J.; Baltrus, J. Experimental and simulation studies on mineral trapping of CO_2 with brine. *Energy Convers. Manag.* **2004**, *45*, 1845–1859. [CrossRef]

58. Xue, W.; Wang, Y.; Chen, Z.; Liu, H. An integrated model with stable numerical methods for fractured underground gas storage. *J. Clean. Prod.* **2023**, *393*, 136268. [CrossRef]

59. Meyer, J.P. *Summary of Carbon Dioxide Enhanced Oil Recovery (CO2 EOR) Injection Well Technology*; American Petroleum Institute: Washington, DC, USA, 2007; Available online: https://www.api.org/~/media/files/ehs/climate-change/summary-carbon-dioxide-enhanced-oil-recovery-well-tech.pdf (accessed on 12 June 2023).